JACS
JOURNAL OF THE AMERICAN CHEMICAL SOCIETY
pubs.acs.org/JACS
Article

Photocatalytic Atomization of the Elemental Species in Solution for Atomic Fluorescence Spectrometry

Lizhen Yan, Wenxi Fang, Huamin Li, Xiaowen Yan, Shi Chen, Limin Yang, and Qiuquan Wang*

Cite This: J. Am. Chem. Soc. 2026, 148, 13682−13688
Read Online
ACCESS | Metrics & More | Article Recommendations | Supporting Information

ABSTRACT: We report a paradigm shift in the atomization of the elemental species in solution using a novel Z-scheme GaP@N-TiO_2 nanocomposite in the presence of formic acid under visible-light irradiation (*vis*-GaP@N-TiO_2−HCOOH), replacing standalone cool diffusion flame-based atomizers presently in use. The atoms formed can be detected in solution by atomic fluorescence spectrometry (*is*AFS) with at least 1 order of magnitude improvement in the limits of detection at the pg mL^{-1} level for As, Se, Hg, Zn, Cd, Ni, Fe, Pb, and Co. During this process, the reductive $CO_2^{\bullet-}$ switched from HCOOH by the valence band h^+ preserved on N-TiO_2 together with the conduction band e^- on GaP plays a synergistic reduction role. Such a new paradigm shift in atomization is expected to challenge the existing norms of atomic spectrometry and give rise to the next-generation *is*AFS and beyond, no longer using the flame atomizer(s), avoiding the use of hazardous chemical(s) and/or harmful UV rays, as well as eliminating the inefficient processes of either sample nebulization and isolation of ultrafine droplets and/or chemical vapor species generated.

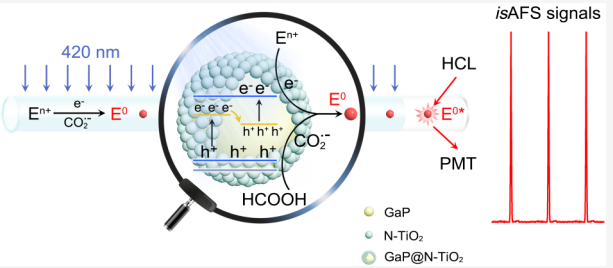

INTRODUCTION

Free atoms are the signal source of atomic spectrometry (AS), which is the most classic and commonly used tool to date for acquiring the most basic information on the elements that make up the objective material world. AS has an unrivaled element-selectivity originating from the quantum leaps of electrons between their intrinsic outer shell orbitals of the atoms. To perform an AS assay, for example, a solution sample is first converted into ultrafine droplets via a pneumatic spray chamber (nebulization), then transported into a standalone high-energy-powered atomizer for atomization in the gaseous phase, and finally determined via optical absorption or emission AS. Unfortunately, the total efficiency of these steps is less than 5% in general, largely impeding the due sensitivity of AS. Pregeneration of chemical vapor species (CVS) from the elemental species (usually a chemical form in which the element exists) using aqueous hydroborates (Scheme 1a),[1] and via the low molecular weight organic acid (LMWOA)-based ultraviolet light (UV)-induced photochemical or nanosemiconductor-based UV-driven photocatalytic strategies,[2−9] remarkably improves the efficiency (Scheme 1b). But the use of hazardous tetrahydroborate (BH_4^-) or harmful UV rays, the inefficient but necessary step for isolation of CVS by a gas−liquid separator, and especially the standalone atomizer(s) of either flame or nonflame are still needed, not to mention being limited to the "vapor-generable" elements. Atomization of the elemental species in solution is therefore much desired to overcome the aforementioned disadvantages. However, few such attempts have been done, except that Ag, Cu, and Pd ions were reduced into free atoms in aqueous solution using $NaBH_4$ and their atomic absorption spectrometric signals were detected.[10,11]

From a chemical perspective, atomization of the elemental species is a reduction process involving the acquisition of electrons. If we are able to provide electrons with enough capability for reduction, atomization of the elemental species should be realized. Fortunately, direct Z-scheme heterojunction nanocomposites[12−14] composed of two sophisticated semiconductor photocatalysts may provide conduction band electrons (CB e^-) with greater reductive ability and valence band holes (VB h^+) with stronger oxidative ability for redox purposes, and more importantly, visible light (*vis*) instead of UV can be utilized depending on the rational design of the nanocomposites. We thus propose to create a novel *vis*-driven GaP@N-TiO_2 from nano gallium phosphide (GaP) and nitrogen-doped titanium dioxide (N-TiO_2), aiming at atomization of the elemental species in solution. As, Se, and Hg species and some other metal ions Zn^{2+}, Cd^{2+}, Ni^{2+}, Fe^{2+}, Co^{2+}, and Pb^{2+} were selected as representatives of the elemental species, and their atoms formed are expected to be detected in solution by atomic fluorescence spectrometry (*is*AFS) (Scheme 1c). We anticipate that this approach will achieve a

Received: November 13, 2025
Revised: March 24, 2026
Accepted: March 25, 2026
Published: March 30, 2026

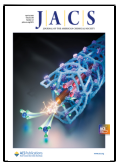

https://doi.org/10.1021/jacs.5c20257
J. Am. Chem. Soc. 2026, 148, 13682−13688

Scheme 1. Atomic Fluorescence Spectrometry[a]

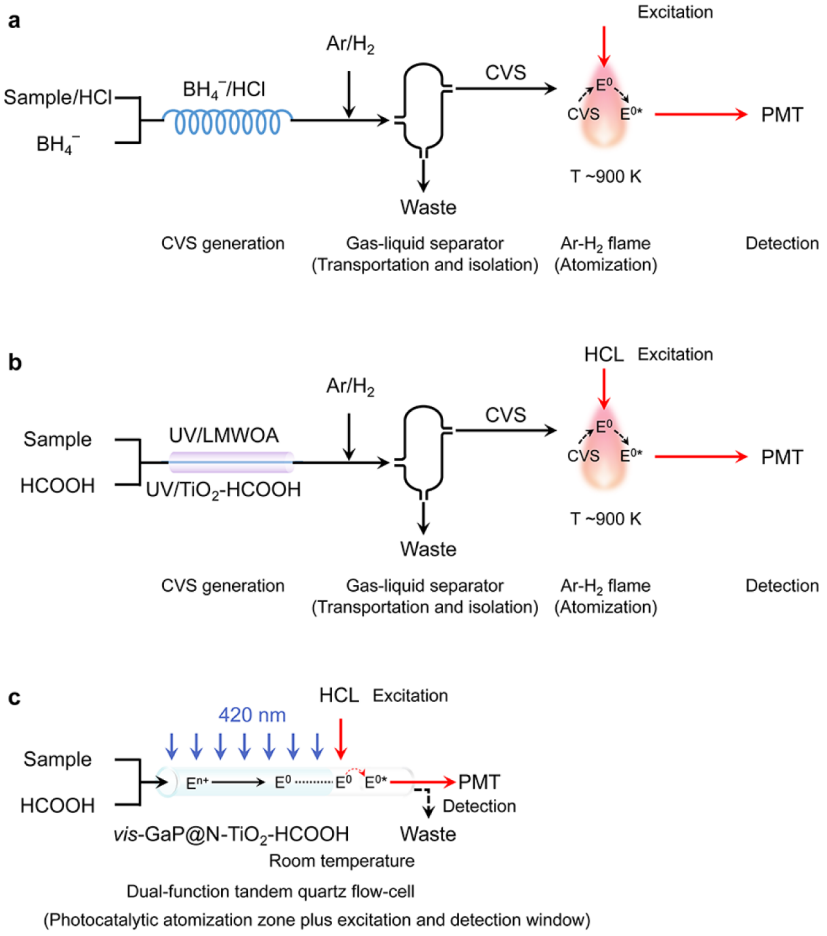

[a](a) Chemical vapor species generation atomic fluorescence spectrometry (CVS-AFS) with an Ar−H_2 flame atomizer: tetrahydroborate-HCl system (BH_4^-/HCl) for hydride generation (HG-AFS); HCL, hollow cathode lamp; PMT, photomultiplier tube. (b) UV-induced low molecular weight organic acid photochemical vapor generation system (UV/LMWOA) and UV-driven nano TiO_2 photocatalytic vapor generation system (UV/TiO_2−HCOOH). (c) This work: visible light-driven HCOOH-mediated GaP@N-TiO_2 photocatalytic atomization of the elemental species in solution atomic fluorescence spectrometry (*vis*-GaP@N-TiO_2−HCOOH-*is*AFS): E^{n+}, elemental species; E^0, ground state atom of the element; E^0*, excited state atom of the element.

new paradigm shift in atomization compared with the conventional techniques and methods, making *is*AFS a simpler, greener, and more sensitive tool for elemental analysis.

RESULTS AND DISCUSSION

Characterization of GaP@N-TiO_2 and Photocatalytic Reduction Mechanism of *vis*-GaP@N-TiO_2−HCOOH

The band gap of GaP prepared (129.6 ± 12.4 nm measured by SEM) was determined to be 2.23 eV between CB −1.33 V vs NHE and VB 0.90 V at pH 3,[15] while that of N-TiO_2 (18.7 ± 2.4 nm with a 0.5 molar ratio of N to Ti) was 2.82 eV between CB −0.15 V and the VB 2.67 V of N-2p, and 3.20 eV between CB −0.15 V and the VB 3.05 V of O-2p (Figure S1), indicating the coexistence of N-2p and O-2p VBs in the N-TiO_2 synthesized.[16,17] GaP and N-TiO_2 prepared have suitable CB and VB energy levels and tend to form a Z-scheme heterostructured nanocomposite, in addition to their stability in acidic media, which is generally required to prevent metals from hydrolysis. The as-prepared GaP@N-TiO_2 (Ga:Ti = 5:100, see the details in Experimental Methods and Supporting Information Figure S1j) was verified by X-ray powder diffractometry (XRD) (Figure 1a and Figure S1e) and energy-dispersive X-ray spectroscopy (EDS) mappings (Figure 1b), indicating that N-TiO_2 still maintains the anatase structure of TiO_2 and GaP has the zinc-blende structure. On the other hand, a clearly direct facet coupling, for example, between N-TiO_2 (101 with the lattice spacing of 0.35 nm) and GaP (111, 0.32 nm) was observed under high-angle annular dark field-scanning transmission electron microscopy (HAADF-STEM) (Figure 1c), suggesting that intimately heterojuncted GaP@N-TiO_2 has been constructed. Moreover, ultraviolet−visible diffuse reflectance spectroscopy (UV−vis DRS) studies (Figure 1d) showed that GaP can be excited by light shorter than 556 nm, and N-TiO_2 by light shorter than 439 nm. These findings imply that GaP@N-TiO_2 is excitable under *vis*-irradiation, such as 420 nm.

Furthermore, electron paramagnetic resonance (EPR) spectroscopic studies (see the experimental details in the Supporting Information) of GaP@N-TiO_2 in pure water (GaP@N-TiO_2−H_2O) under 365 and 420 nm irradiation showed a typical four-line spectrum of ·OH-DMPO spin adduct[18] under 365 nm irradiation (Figure 2a) but not under 420 nm (Figure 2b), because only 365 nm is capable of photogenerating O-2p VB h^+ (3.05 V) that is able to oxidize

https://doi.org/10.1021/jacs.5c20257
J. Am. Chem. Soc. 2026, 148, 13682−13688

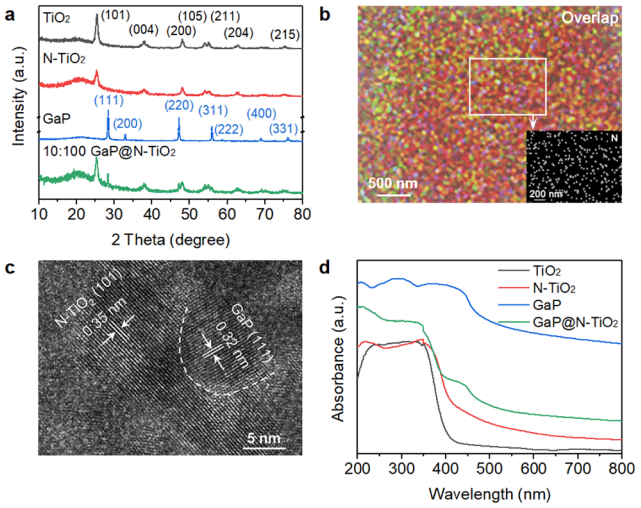

Figure 1. Characterization of TiO_2, N-TiO_2, GaP, and GaP@N-TiO_2. (a) XRD of TiO_2, N-TiO_2, GaP, and GaP@N-TiO_2 (Ga:Ti = 5:100). (b) EDS element mapping of Ti (red), O (green), N (inset, gray), Ga (yellow), and P (blue) of GaP@N-TiO_2. (c) HAADF-STEM image of GaP@N-TiO_2. (d) UV−vis DRS of TiO_2, N-TiO_2, GaP, and GaP@N-TiO_2.

H_2O into ·OH ($E^0_{\cdot OH/H_2O} = +2.7$ V).[19] This phenomenon observed verifies that GaP@N-TiO_2 is a typical Z-scheme heterojunction nanocomposite, not a Type-II system that transfers the VB h^+ of N-TiO_2 to the lower VB (0.90 V) of GaP. When adding HCOOH into the above system (GaP@N-TiO_2−HCOOH), ·OH disappears while $CO_2^{\bullet-}$ appears with the characteristic DMPO−$CO_2^{\bullet-}$ spin adduct[20] under 365 nm irradiation (Figure 2a), implying that either the strong oxidative ·OH was consumed by HCOOH ($E^0_{CO_2^{\cdot-}/HCOOH} = +1.07$ V)[21] into the reductive radical $CO_2^{\bullet-}$ ($E^0_{CO_2/CO_2^{\cdot-}} = -2.00$ V),[22] or the 365 nm-photogenerable O-2p and N-2p VB h^+ oxidized HCOOH directly into $CO_2^{\bullet-}$, blocking the formation of ·OH from H_2O. More excitingly, $CO_2^{\bullet-}$ was also observed under 420 nm irradiation (Figure 2b), indicating that the 420 nm-photogenerable N-2p VB h^+ (2.67 V) can oxidize HCOOH into $CO_2^{\bullet-}$. This is vital for harboring the electrons in *vis*-GaP@N-TiO_2−HCOOH system, in which the concomitantly existing yet innately contradictory oxidative VB h^+ and reductive CB e^- are harmonized by HCOOH. The HCOOH-mediated switch of the oxidative h^+ to the reductive $CO_2^{\bullet-}$ lays the basis for the atomization of elemental species in solution (Figure 2e).

Using H_3AsO_3 (As^{III}) and $H_2AsO_4^-$ (As^V) as the representative elemental species to probe the efficacy of *vis*-GaP@N-TiO_2−HCOOH, the formation of As^0 was confirmed by its atomic fluorescent signals using As HCL as the excitation source (Figure 2c) and EDS (Figure 2d). Meanwhile, the significant decrease in the signal intensity of DMPO−$CO_2^{\bullet-}$ after the addition of As^{III} (Figure 2a and b) witnesses the participation of $CO_2^{\bullet-}$ in the atomization process of As^{III} to As^0 ($E^0_{As^{III}/As^0} = +0.24$ V).[23] While using As^V and CH_3CH_2OH instead of HCOOH (*vis*-GaP@N-TiO_2−CH_3CH_2OH), the produced $CH_3\dot{C}HOH$ radical ($E^0_{CH_3\dot{C}HOH/CH_3CHO} = -1.18$ V)[24] hardly overcomes the energy barrier of As^V to As^{IV} ($E^0_{As^V/As^{IV}} = -1.2$ V),[25] and thus finds it difficult to undergo the subsequent processes of reducing As^V

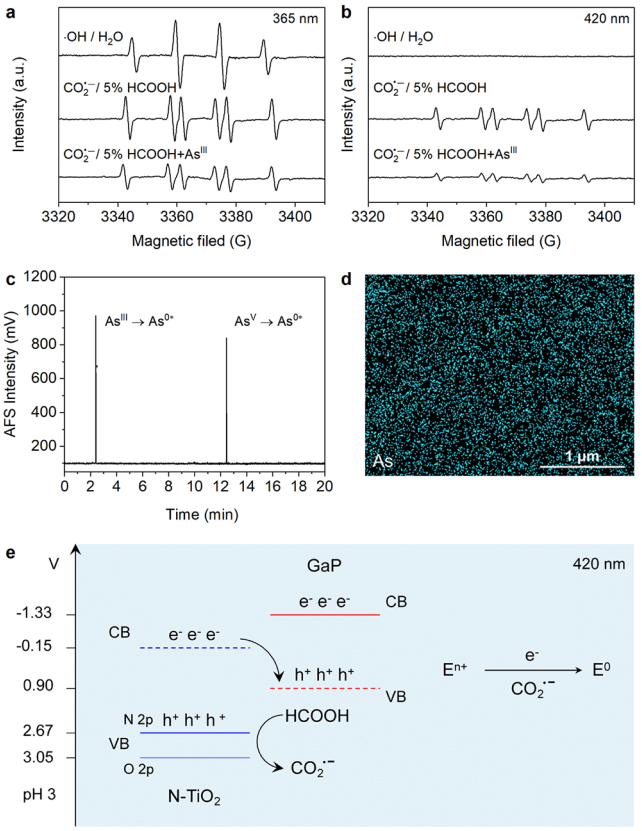

Figure 2. EPR of •OH and $CO_2^{\bullet-}$ in GaP@N-TiO_2−H_2O, GaP@N-TiO_2−HCOOH, and GaP@N-TiO_2−HCOOH-As^{III} systems under 365 nm (a) and 420 nm (b) irradiation. •OH-DMPO in GaP@N-TiO_2−H_2O system under 365 nm irradiation: the intensity ratio 1:2:2:1, g-factor 2.006, and hyperfine constants α_N = 14.9 G and α_H = 14.9 G; DMPO−$CO_2^{\bullet-}$ in GaP@N-TiO_2−HCOOH system: the intensity ratio 1:1:1:1:1:1, g-factor 2.006, and hyperfine constants α_N = 15.3 G and α_H = 18.7 G. (c) *is*AFS of As^0 atomized from As^{III} and As^V (10 ng each) by *vis*-GaP@N-TiO_2−HCOOH (2.5% HCOOH, pH 3) under 420 nm irradiation. (d) EDS of As on the GaP@N-TiO_2 surface. (e) Photocatalytic reduction mechanism of *vis*-GaP@N-TiO_2−HCOOH (2.5% HCOOH, pH 3) under 420 nm irradiation for reducing E^{n+} to E^0 in solution.

to As^0. Nevertheless, the relatively weak atomic fluorescent signals of As^0 were still detected in this case (Figure S2), indicating that the CB e^- (−1.33 V) preserved on GaP@N-TiO_2 can independently fulfill the task of As^V to As^0. These results further evidence that GaP@N-TiO_2 is a Z-scheme heterojunction nanocomposite and not a type-II system that transfers the CB e^- on GaP to the lower CB (−0.15 V) of N-TiO_2, suggesting that the strong reducing radical $CO_2^{\bullet-}$ switched from HCOOH by the oxidative VB h^+ together with the CB e^- play a synergistic role in the atomization of As species in solution (Figure 2e). Moreover, it should be pointed out that the As^0 formed can be reduced further to volatile AsH_3 ($E^0_{As^0/AsH_3} = -0.23$ V).[23] This was not only evidenced by the AFS signals detected in an Ar−H_2 flame after isolation of AsH_3 via a gas−liquid separator when applying a longer irradiation time (23.6 s) (*vis*-GaP@N-TiO_2−HCOOH-(AsH_3/Ar−H_2)-AFS) (Figure S3), but also identified by GC-MS after collection (7 h) using a glass wool-packed U-tube immersed in a liquid-N_2 cold trap (−196 °C) (Figure S4). These findings suggest that As^0 is just an intermediate before finally forming

https://doi.org/10.1021/jacs.5c20257
J. Am. Chem. Soc. 2026, 148, 13682−13688

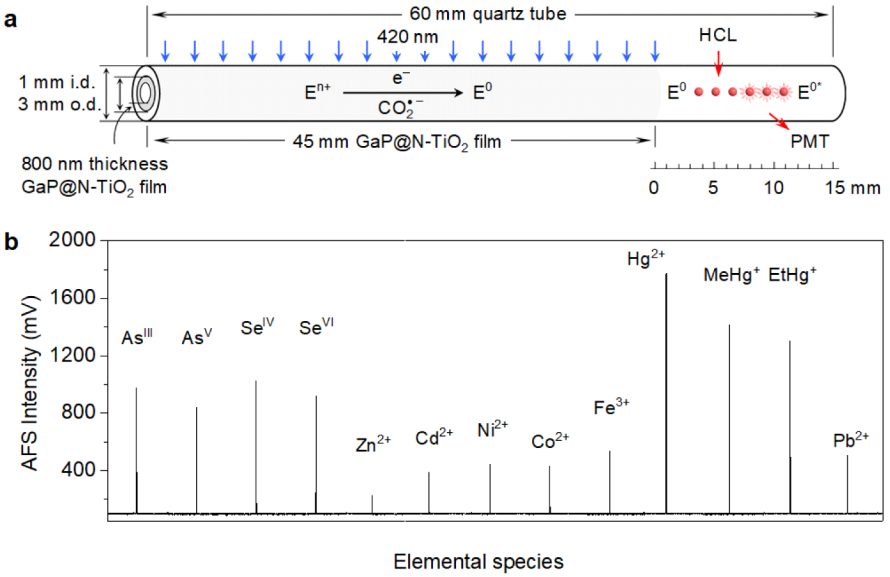

Figure 3. (a) Schematic diagram of the tandem reduction-detection flow-cell for *vis*-GaP@N-TiO_2−HCOOH-*is*AFS. (b) *is*AFS signals of As^{III}, As^V, Se^{IV}, Se^{VI}, Hg^{2+}, $MeHg^+$, $EtHg^+$, Ni^{2+}, Cd^{2+}, Zn^{2+}, Fe^{3+}, Pb^{2+}, and Co^{2+} (10 ng each) with 2.5% HCOOH (pH 3) at a flow rate of 0.4 mL min^{-1} under 420 nm irradiation.

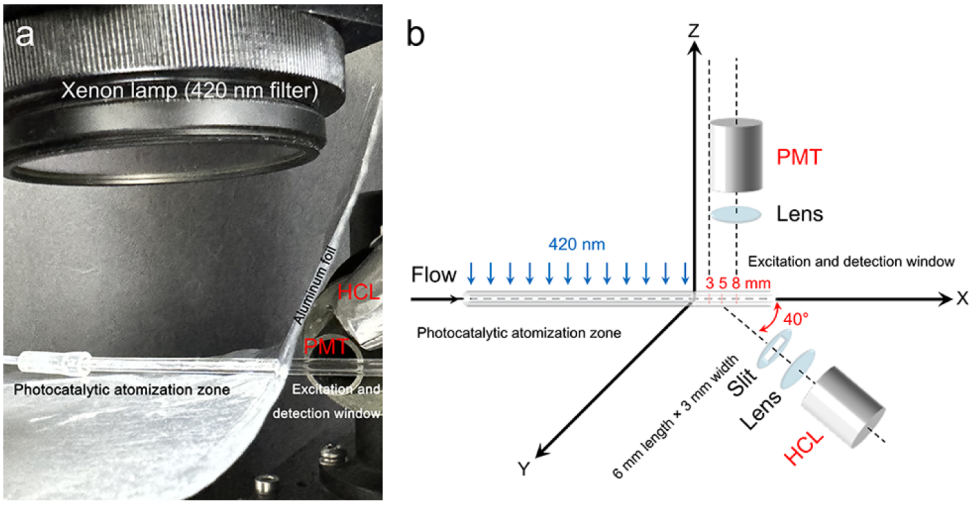

Figure 4. (a) Photo and (b) diagram of *vis*-GaP@N-TiO_2−HCOOH-*is*AFS platform focusing on the tandem reduction-detection dual-function flow-cell and the arrangement of the xenon lamp with a 420 nm optical filter, HCL, and PMT.

AsH_3 in the *vis*-GaP@N-TiO_2−HCOOH system. The half-life of As^0 was determined to be 1.9 s according to the logarithmic AFS intensity over time (Figure S5), implying that the design of a suitable tandem reduction-detection dual-function flow-cell is very important for *is*AFS.

vis-GaP@N-TiO_2−HCOOH-*is*AFS and Its Performance

We designed and made a quartz flow-cell with dimensions of 1.0 mm i.d. × 3.0 mm o.d. × 60 mm in length (Figure 3a). On the inner surface of its preceding 45 mm, an 800 nm thick GaP@N-TiO_2 layer (Figure S 1d) was sintered, while the subsequent 15 mm was left as a transparent window for *is*AFS. Using As HCL (Beijing General Research Institute for Nonferrous Metals, China) to excite the As^0 formed from As^{III} and/or As^V, the fluorescent signals emitted from the excited As^{0*} were collected by a sunblind photomultiplier tube (PMT R7154, 160−320 nm, Hamamatsu, Japan) (Figure 3b). Under the optimum conditions of 5.3 s 420 nm irradiation from a xenon lamp equipped with a 420 nm optical filter (300 W CME-Xe300F, Beijing Zhongke Weineng Technology Co. Ltd., China) and 2.5% HCOOH with a flow rate of 0.4 mL min^{-1} (Figure 4, and see the optimization details in Supporting Information, Table S1 and Figures S6−S8), the LODs (3σ) of As^{III} and As^V obtained were 2.23 and 2.45 pg mL^{-1} with the RSDs of 2.37% and 2.68% at 100 ng mL^{-1} (n = 7), and the linear range of their calibration curves extended up to 1000 ng mL^{-1} with a regression coefficient (R^2) greater than 0.998 (Figure S9a). Higher concentrations were not tested considering that higher concentrations would cause the coalescence of free atoms to form nanoparticles,[26] thereby affecting the AFS detection. These LODs are 19 and 25 times lower than those of 42.5 pg mL^{-1} As^{III} and 62.3 pg mL^{-1} As^V obtained by the conventional HG-AFS using $NaBH_4$ (Scheme 1a and Table S1), and 37 and 40 times lower than 83.6 pg mL^{-1} As^{III} and 98.1 pg mL^{-1} As^V obtained using *vis*-GaP@N-TiO_2−HCOOH-(AsH_3/Ar−H_2)-AFS (Table S1 and Figure

https://doi.org/10.1021/jacs.5c20257
J. Am. Chem. Soc. 2026, 148, 13682−13688

S3). We speculate that the improvements in the LODs of *is*AFS are mostly ascribed to the elimination of the dilution effect during the transportation of CVS and in the Ar−H_2 flame, although the collision quenching in solution should be much more significant than that in the flame. After validation by quantifying the total As content in the standard water reference material GBW-08666 (Table S2), *vis*-GaP@N-TiO_2−HCOOH-*is*AFS was applied to the determination of the total As in real-world kelp samples. The As concentration of 11.6 ± 0.35 mg kg^{-1} determined in the kelp samples (n = 7) was well in agreement with 11.5 ± 0.18 mg kg^{-1} (n = 7) obtained with the Chinese National Standard HG-AFS Method[27] (Table S2, and see the detailed sample pretreatment method in the Supporting Information), indicating that *vis*-GaP@N-TiO_2−HCOOH-*is*AFS was accurate and practical.

To expand the feasibility of *vis*-GaP@N-TiO_2−HCOOH-*is*AFS toward other elements, Se, Hg, Ni, Cd, Zn, Fe, Pb, and Co were preliminarily investigated under the same conditions as those for As, except for using their respective HCLs (Table S1 and Figure 3b). Their LODs (3σ) reach 1.15 ($HSeO_3^-$, Se^{IV}), 1.22 (SeO_4^{2-}, Se^{VI}), 0.43 (Hg^{2+}), 0.52 ($MeHg^+$), 0.54 ($EtHg^+$), 4.72 (Ni^{2+}), 5.18 (Cd^{2+}), 6.42 (Zn^{2+}), 4.26 (Fe^{3+}), 4.40 (Pb^{2+}), and 4.80 (Co^{2+}) pg mL^{-1}, respectively, with the RSDs of lower than 2.73% at 100 ng mL^{-1} (n = 7), and the linear range of their calibration curves up to 1000 ng mL^{-1} (higher concentrations were not tested) with R^2 greater than 0.997 (Figure S9b−i). Such LODs of the elemental species investigated here generally correspond to their redox potentials[2,3] ($E^0_{HSeO_3^-/Se^0} = 0.78$ V; $E^0_{SeO_4^{2-}/Se^0} = 0.88$ V; $E^0_{Hg^{2+}/Hg^0} = 0.85$ V; $E^0_{Ni^{2+}/Ni^0} = -0.26$ V; $E^0_{Cd^{2+}/Cd^0} = -0.40$ V; $E^0_{Zn^{2+}/Zn^0} = -0.76$ V; $E^0_{Fe^{3+}/Fe^0} = -0.04$ V; $E^0_{Pb^{2+}/Pb^0} = -0.13$ V; and $E^0_{Co^{2+}/Co^0} = -0.28$ V); however, it should be noted that the surface of GaP@N-TiO_2 at pH 3 is positively charged considering its point of zero charge pH is 5.2 (Figure S1h). The positively charged surface may attract negatively charged ions such as $H_2AsO_4^-$ (As^V), $HSeO_3^-$ (Se^{IV}), and SeO_4^{2-} (Se^{VI}), while repelling the positively charged Hg^{2+}, $MeHg^+$, $EtHg^+$, Ni^{2+}, Cd^{2+}, Zn^{2+}, Fe^{3+}, Pb^{2+}, and Co^{2+} to some extent, resulting in their compromised LODs. But even so, their LODs are still at least 1 order of magnitude superior to those reported using optical AS and comparable to those obtained by direct-injection inductively coupled plasma mass spectrometry. Moreover, the speciation analysis of As (Figure S10a), Se (Figure S10b), and Hg (Figure S10c) can be accomplished when coupling with HPLC (Table S3), suggesting that *vis*-GaP@N-TiO_2−HCOOH-*is*AFS can be adopted as an HPLC detector. However, it should be noted that the peak widths determined are much shorter than we expected. These phenomena observed might be due to the possible formation of the nanoclusters and/or the CVS of the elements tested, and the kinetics behind them remain to be further explored.

CONCLUSIONS

We developed a *vis*-GaP@N-TiO_2−HCOOH photocatalytic approach for the atomization of the elemental species in solution, replacing the standalone cool diffusion flame-based atomizer(s) currently in use, while improving the LODs for As, Se, Hg, Ni, Cd, Zn, Fe, Pb, and Co by more than 1 order of magnitude at the pg mL^{-1} level using *vis*-GaP@N-TiO_2−HCOOH-*is*AFS. Besides being able to do what the currently most popular HG-AFS did, as well as being a greener or more sustainable one, *vis*-GaP@N-TiO_2−HCOOH-*is*AFS has no requirement for whether an element can be transformed into CVS or not, implying that more elements can be determined as long as they can be atomized in solution. Moreover, the relatively cumbersome and inefficient yet necessary procedures of generation, isolation, transportation, as well as atomization of CVS for a targeted element in HG-AFS can be excluded; the corresponding order-of-magnitude dilution effect on the CVS during these processes can be thus overcome by *vis*-GaP@N-TiO_2−HCOOH-*is*AFS, lowering the limit of detection and further improving sensitivity. We believe such a new paradigm shift in atomization will trigger a revolution in the field of optical AS and give birth to next-generation *is*AFS with the characteristics of energy-saving, simple instrumentation and green methods for the determination of more elements in the Periodic Table of the Elements (Figure S11). Nevertheless, it should be pointed out that the strongest reductive species involved in *vis*-GaP@N-TiO_2−HCOOH-*is*AFS for the atomization of the elemental species is the $CO_2^{\bullet-}$ radical converted from HCOOH by the VB h^+; its reducing power is still far from sufficient for the atomization of alkali metals, alkaline earth metals, and lanthanides as well. On the other hand, the photoredox catalysts with more negative CB e^- should benefit the improvement in the reducing ability. Thus, further efforts to discover both novel precursor compounds of stronger reducing radicals and photoredox catalysts with more negative CB e^- hold significant promise.

EXPERIMENTAL METHODS

Preparation of GaP@N-TiO_2 and Tandem Reduction-Detection Dual-Function Flow-Cell

We started with the synthesis of nano GaP and N-TiO_2 to build a GaP@N-TiO_2 nanocomposite. Briefly, nano N-TiO_2 was prepared by a sol−gel method[3,6] with some modifications using titanium tetraisopropoxide as the titanium source, urea as the nitrogen source, and acetylacetone as the stabilizer in anhydrous ethanol. To prepare nano GaP, we first used anhydrous gallium chloride ($GaCl_3$) to react with sodium phosphide (Na_3P) in distilled dimethylbenzene under an anhydrous and oxygen-free atmosphere to produce a black solid product.[28] This product was then heated to 600 °C at a rate of 10 °C min^{-1} and kept for 1 h in a tube furnace under an argon atmosphere, obtaining a brown product. After it was soaked in hydrochloric acid for 12 h to remove the possible byproduct $GaPO_4$, washed with ultrapure water to neutrality, and dried under vacuum at 40 °C, we finally obtained deep green GaP nanoparticles (see the experimental details in Supporting Information). Subsequently, we prepared the GaP@N-TiO_2 nanocomposite by dispersing GaP into the sol of N-TiO_2 followed by calcination at 450 °C for 1 h (see the experimental details in Supporting Information).

In parallel, the GaP@N-TiO_2 sol was injected into the quartz tube [1 mm i.d. × 3 mm o.d. × 60 mm in length; pretreatment of the quartz tube (JGS1, Beijing Jinghui Wanbo Technology Co., Ltd.) is described in the Supporting Information] until 45 mm via a syringe, and the remaining 15 mm was kept transparent as the excitation and detection window for *is*AFS. After being maintained inside the tube for 10 min, the sol was purged out of the tube in the reverse direction using an Ar gas flow. Subsequently, the tube was dried at 80 °C for 30 min in an electric oven, then transferred to a muffle furnace, and calcined at a gradually increasing temperature of 1.5 °C min^{-1} to 450 °C and kept for 1 h. These procedures were repeated 5 times to obtain an 800 nm film of GaP@N-TiO_2 on the inner surface of the quartz tube. The obtained dual-function flow-cell was washed using UPW and dried at 80 °C before use.

https://doi.org/10.1021/jacs.5c20257
J. Am. Chem. Soc. 2026, 148, 13682−13688

vis-GaP@N-TiO_2–HCOOH-*is*AFS Platform

We adapted the optical system of AFS-9750 (Beijing Haiguang Instrument Co., Ltd.) and its operation and data processing software (Analyzer Software V2.0.01) to construct *vis*-GaP@N-TiO_2–HCOOH-*is*AFS platform with some modifications, as shown in Figure 4. Keeping the angle of incidence of the HCL at 40°, we can obtain optimal AF signals when the distance is 3 mm between the center of the circular window of the PMT and the center of the light spot from the HCL on the *X*-axis, during which the HCL and PMT are aligned at 90°. In this situation, the window of the PMT and the light spot from the HCL are partly overlapped, and the excitation from the HCL and the signal acquisition by the PMT are controlled simultaneously as well.

■ ASSOCIATED CONTENT

Supporting Information

The Supporting Information is available free of charge at https://pubs.acs.org/doi/10.1021/jacs.5c20257.

Experimental details for the synthesis and characterization of GaP@N-TiO_2 nanocomposite and studies of its photocatalytic behaviors including EPR experiments, as well as the instrumentation of *vis*-GaP@N-TiO_2–HCOOH-*is*AFS and optimization of its operating conditions including slit size, irradiation time, HCL current, PMT negative high voltage, and the effect of HCOOH concentration; method validation and sample analysis; As, Se, and Hg speciation analysis; the elements that can be detected by *vis*-GaP@N-TiO_2–HCOOH-*is*AFS and those predicted to be detected in the Periodic Table of the Elements (PDF)

■ AUTHOR INFORMATION

Corresponding Author

Qiuquan Wang − *Department of Chemistry & the MOE Key Laboratory of Spectrochemical Analysis and Instrumentation, College of Chemistry and Chemical Engineering, Xiamen University, Xiamen 361005, China*; orcid.org/0000-0002-5166-4048; Email: qqwang@xmu.edu.cn

Authors

Lizhen Yan − *Department of Chemistry & the MOE Key Laboratory of Spectrochemical Analysis and Instrumentation, College of Chemistry and Chemical Engineering, Xiamen University, Xiamen 361005, China*

Wenxi Fang − *Department of Chemistry & the MOE Key Laboratory of Spectrochemical Analysis and Instrumentation, College of Chemistry and Chemical Engineering, Xiamen University, Xiamen 361005, China*

Huamin Li − *Department of Chemistry & the MOE Key Laboratory of Spectrochemical Analysis and Instrumentation, College of Chemistry and Chemical Engineering, Xiamen University, Xiamen 361005, China*

Xiaowen Yan − *Department of Chemistry & the MOE Key Laboratory of Spectrochemical Analysis and Instrumentation, College of Chemistry and Chemical Engineering, Xiamen University, Xiamen 361005, China*; orcid.org/0000-0001-6608-6044

Shi Chen − *Department of Chemistry & the MOE Key Laboratory of Spectrochemical Analysis and Instrumentation, College of Chemistry and Chemical Engineering, Xiamen University, Xiamen 361005, China*

Limin Yang − *Department of Chemistry & the MOE Key Laboratory of Spectrochemical Analysis and Instrumentation, College of Chemistry and Chemical Engineering, Xiamen University, Xiamen 361005, China*

Complete contact information is available at: https://pubs.acs.org/10.1021/jacs.5c20257

Notes

The authors declare no competing financial interest.

■ ACKNOWLEDGMENTS

This work was supported by the National Natural Science Foundation of China (No. 22193053, 22576171, and 21535007). We thank Jing Liang and Junyu Wang of Beijing Haiguang Instrument Co., Ltd. for their assistance to build the optical platform. Thanks also go to the anonymous reviewers for their professional and constructive comments during the revision of this article.

■ REFERENCES

(1) D'Ulivo, A.; Dědina, J.; Mester, Z.; Sturgeon, R. E.; Wang, Q.; Welz, B. Mechanisms of chemical generation of volatile hydrides for trace element determination (IUPAC Technical Report). *Pure Appl. Chem.* **2011**, *83*, 1283−1340.

(2) Guo, X.; Sturgeon, R. E.; Mester, Z.; Gardner, G. J. UV Vapor Generation for Determination of Selenium by Heated Quartz Tube Atomic Absorption Spectrometry. *Anal. Chem.* **2003**, *75*, 2092−2099.

(3) Wang, Q.; Liang, J.; Qiu, J.; Huang, B. Online Pre-Reduction of Selenium(VI) with a Newly Designed UV/TiO_2 Photocatalysis Reduction Device. *J. Anal. At. Spectrom.* **2004**, *19*, 715−716.

(4) Zheng, C.; Li, Y.; He, Y.; Ma, Q.; Hou, X. Photo-Induced Chemical Vapor Generation with Formic Acid for Ultrasensitive Atomic Fluorescence Spectrometric Determination of Mercury: Potential Application to Mercury Speciation in Water. *J. Anal. At. Spectrom.* **2005**, *20*, 746−750.

(5) Yin, Y.; Liang, J.; Yang, L.; Wang, Q. Vapour Generation at a UV/TiO_2 Photocatalysis Reaction Device for Determination and Speciation of Mercury by AFS and HPLC-AFS. *J. Anal. At. Spectrom.* **2007**, *22*, 330−334.

(6) Li, H.; Luo, Y.; Li, Z.; Yang, L.; Wang, Q. Nanosemiconductor-Based Photocatalytic Vapor Generation Systems for Subsequent Selenium Determination and Speciation with Atomic Fluorescence Spectrometry and Inductively Coupled Plasma Mass Spectrometry. *Anal. Chem.* **2012**, *84*, 2974−2981.

(7) Sturgeon, R. E. Photochemical Vapor Generation: a Radical Approach to Analyte Introduction for Atomic Spectrometry. *J. Anal. At. Spectrom.* **2017**, *32*, 2319−2340.

(8) Li, H.; Xu, Z.; Yang, L.; Wang, Q. Determination and Speciation of Hg Using HPLC-AFS by Atomization of This Metal on a UV/nano-ZrO_2/HCOOH Photocatalytic Reduction Unit. *J. Anal. At. Spectrom.* **2015**, *30*, 916−921.

(9) Jeníková, E.; Vyhnanovský, J.; Hašlová, K.; Sturgeon, R. E.; Musil, S. Efficient Photochemical Vapor Generation from Low Concentration Formic Acid Media. *Anal. Chem.* **2024**, *96*, 1241−1250.

(10) Panichev, N.; Sturgeon, R. E. Atomic Absorption by Free Atoms in Solution Following Chemical Reduction from the Ionic State. *Anal. Chem.* **1998**, *70*, 1670−1676.

(11) Molloy, J. L.; Holcombe, J. A. Detection of Palladium by Cold Atom Solution Atomic Absorption. *Anal. Chem.* **2006**, *78*, 6634−6639.

(12) Yu, J.; Wang, S.; Low, J.; Xiao, W. Enhanced Photocatalytic Performance of Direct Z-Scheme g-C_3N_4−TiO_2 Photocatalysts for the Decomposition of Formaldehyde in Air. *Phys. Chem. Chem. Phys.* **2013**, *15*, 16883−16890.

(13) Low, J.; Jiang, C.; Cheng, B.; Wageh, S.; Al-Ghamdi, A. A.; Yu, J. A Review of Direct Z-Scheme Photocatalysts. *Small Methods* **2017**, *1* (5), 1700080.

(14) Gu, C.; Hisatomi, T.; Takata, T.; Domen, K. Z-Scheme Water Splitting Systems Based on Solid-State Electron Conductors. *Adv. Funct. Mater.* **2026**, *36* (21), 2506171.
(15) Madelung, O. *Semiconductors Data Handbook*, 3rd ed.; Springer: Berlin Heidelberg, 2004.
(16) Nakamura, R.; Tanaka, T.; Nakato, Y. Mechanism for Visible Light Responses in Anodic Photocurrents at N-Doped TiO_2 Film Electrodes. *J. Phys. Chem. B* **2004**, *108*, 10617−10620.
(17) Asahi, R.; Morikawa, T.; Irie, H.; Ohwaki, T. Nitrogen-Doped Titanium Dioxide as Visible-Light-Sensitive Photocatalyst: Designs, Developments, and Prospects. *Chem. Rev.* **2014**, *114*, 9824−9852.
(18) Barroso-Martínez, J. S.; Romo, A. I. B.; Pudar, S.; Putnam, S. T.; Bustos, E.; Rodríguez-López, J. Real-Time Detection of Hydroxyl Radical Generated at Operating Electrodes via Redox-Active Adduct Formation Using Scanning Electrochemical Microscopy. *J. Am. Chem. Soc.* **2022**, *144*, 18896−18907.
(19) Wardman, P. Reduction Potentials of One-Electron Couples Involving Free Radicals in Aqueous Solution. *J. Phys. Chem. Ref. Data* **1989**, *18*, 1637−1755.
(20) Perissinotti, L. L.; Brusa, M. A.; Grela, M. A. Yield of Carboxyl Anion Radicals in the Photocatalytic Degradation of Formate over TiO_2 Particles. *Langmuir* **2001**, *17*, 8422−8427.
(21) Koppenol, W. H.; Rush, J. D. Reduction Potential of the Carbon Dioxide/Carbon Dioxide Radical Anion: a Comparison with Other C1 Radicals. *J. Phys. Chem.* **1987**, *91*, 4429−4430.
(22) Leonori, D.; Sturgeon, R. E. A Unified Approach to Mechanistic Aspects of Photochemical Vapor Generation. *J. Anal. At. Spectrom.* **2019**, *34*, 636−654.
(23) *Standard Potentials in Aqueous Solutions*, Bard, A. J.; Parsons, R.; Jordan, J., Eds.; Routledge: New York, 1985.
(24) Schneider, J.; Matsuoka, M.; Takeuchi, M.; Zhang, J.; Horiuchi, Y.; Anpo, M.; Bahnemann, D. W. Understanding TiO_2 Photocatalysis: Mechanisms and Materials. *Chem. Rev.* **2014**, *114*, 9919−9986.
(25) Kläning, U. K.; Bielski, B. H. J.; Sehested, K. Arsenic (IV) A Pulse-radiolysis Study. *Inorg. Chem.* **1989**, *28*, 2717−2724.
(26) Sturgeon, R. E.; Pagliano, E.; Lopes, G. S.; Neto, R. S. A.; Brito, J. K. S. Insights into the Role of Transition and Noble Metals Mediating Photochemical Vapor Generation. *J. Anal. At. Spectrom.* **2025**, *40*, 70−97.
(27) National Health Commission of the People's Republic of China State Administration for MarketRegulation *Determination of Total Arsenic and Inorganic Arsenic in Food; GB 5009.11−2024*; National Health Commission of the PRC: Beijing, 2024.
(28) Zhang, Z. C.; Wang, B. P. Diamond and Oxidized Disordered Graphite on the Surface of Gallium Phosphide Nanoparticles. *Part. Part. Syst. Charact.* **2009**, *26*, 53−57.

https://doi.org/10.1021/jacs.5c20257
J. Am. Chem. Soc. 2026, 148, 13682−13688